



## Inductively Coupled Plasma Etching of Bulk Titanium for MEMS Applications

E. R. Parker,<sup>a,\*</sup> B. J. Thibeault,<sup>b</sup> M. F. Aimi,<sup>c</sup> M. P. Rao,<sup>a</sup> and N. C. MacDonald<sup>a,c</sup>

<sup>a</sup>Department of Mechanical and Environmental Engineering, <sup>b</sup>Department of Electrical and Computer Engineering, and <sup>c</sup>Department of Materials, University of California, Santa Barbara, Santa Barbara, California 93106

Titanium is a promising new material system for the bulk micromachining of microelectromechanical (MEMS) devices. Titanium-based MEMS have the potential to be used for a number of applications, including those which require high fracture toughness or biocompatibility. The bulk titanium etch rate, TiO<sub>2</sub> mask etch rate, and surface roughness in an inductively coupled plasma (ICP) as a function of various process parameters are presented. Optimized conditions are then used to develop the titanium ICP deep etch (TIDE) process. The TIDE process is capable of producing high aspect ratio structures with smooth sidewalls at etch rates in excess of 2 μm/min, providing a new means for the microfabrication of titanium-based MEMS devices.  
© 2005 The Electrochemical Society. [DOI: 10.1149/1.2006647] All rights reserved.

Manuscript submitted January 19, 2005; revised manuscript received May 6, 2005. Available electronically August 12, 2005.

Traditionally, microelectromechanical systems (MEMS) have relied heavily on materials used in integrated circuit fabrication, such as single-crystal silicon. However, due to the mechanical nature of some MEMS devices, performance may be limited by the intrinsic properties of these materials. Therefore, additional material systems such as metals are being considered as potential candidates for bulk MEMS because their relative ductility may reduce the risk of failure associated with brittle silicon.<sup>1</sup> Recent developments have allowed for the realization of bulk titanium MEMS for devices that require higher fracture toughness and/or resistance to harsh environments.<sup>2</sup> Titanium may also serve as a potential substrate for in vivo applications given its excellent biocompatibility.<sup>3</sup> However, for bulk titanium MEMS to become a competitive alternative to traditional silicon-based devices, high etch rates, high aspect ratios, and high mask selectivity are essential. This paper reports on the development of a high aspect ratio titanium micromachining method, the titanium ICP deep etch (TIDE) process, which satisfies these requirements.

To date, the majority of research on titanium dry etching has been performed on deposited thin films and implements fluorine- and/or chlorine-based chemistries.<sup>4-8</sup> Reported gases suitable for titanium etching include: CCl<sub>4</sub>/O<sub>2</sub> with additions of fluorine-containing gases;<sup>4</sup> CCl<sub>4</sub>/CCl<sub>2</sub>F<sub>2</sub> with admixtures of O<sub>2</sub>;<sup>5</sup> Cl<sub>2</sub>/BCl<sub>3</sub>;<sup>6</sup> Cl<sub>2</sub>/N<sub>2</sub>;<sup>7</sup> CF<sub>4</sub>, CF<sub>4</sub>/O<sub>2</sub>, SiCl<sub>4</sub>, SiCl<sub>4</sub>/CF<sub>4</sub>, and CHF<sub>3</sub>;<sup>8</sup> CF<sub>4</sub>/O<sub>2</sub>;<sup>9</sup> and SF<sub>6</sub>.<sup>10</sup> Although titanium thin films are commonly used in microelectronics, micromechanical structures dry etched into titanium thin films have only recently been demonstrated.<sup>11</sup> However, because thin films limit aspect ratio and often contain residual stresses, bulk titanium may be a more suitable option for certain MEMS applications.

Dry etching of high aspect ratio structures in bulk titanium using a cyclic Cl<sub>2</sub>/Ar process has been demonstrated by the metal anisotropic reactive ion etching with oxidation (MARIO) process, but with relatively low etch rates due to the parallel plate system being used.<sup>2</sup> This work reports the characterization of bulk titanium deep etching using Cl<sub>2</sub>/Ar chemistry with an inductively coupled plasma (ICP) source. Titanium etch rate, etch rate of a TiO<sub>2</sub> masking layer, and roughness of the etched surface have been studied over a large parameter space on patterned samples. The ICP source power, sample rf power, process pressure, and gas flow rates were varied individually and plotted to determine first-order trends associated with each parameter. Based on the results of this etch characterization, parameters were optimized to develop the titanium ICP deep etch (TIDE) process for etching high aspect ratio microstructures in thick titanium substrates. Bulk titanium etch rates in excess of 2 μm/min with high TiO<sub>2</sub> mask selectivity (40:1, Ti:TiO<sub>2</sub>) were realized. The TIDE process can also be used to etch thin titanium

foils. These foils can then be bonded to form 3D devices with arbitrary cross sections.<sup>2</sup> Furthermore, unlike the MARIO process, the TIDE process is noncyclic and results in smooth sidewalls due to the elimination of sidewall scalloping.

### Experimental

Two different titanium material types were used for this set of experiments. Commercially pure Grade 1 titanium sheets with polished finish (Tokyo Stainless Grinding Co., Ltd, Tokyo, Japan) approximately 500 μm thick were purchased and used for the etch characterization and high aspect ratio etching. These substrates were sectioned into 2.5 × 2.5 cm samples using a mechanical shearing tool (24-in. Bench-Top square cut shears, McMaster-Carr, Los Angeles, CA). Titanium thin foils (2.5 × 2.5 cm, 99.6% annealed, Goodfellow Corporation, Devon, PA) were also purchased and used for the thin-foil etching experiments. These foils ranged in thickness from 10 to 100 μm and required chemical mechanical polishing (MultiPrep System, Allied High Tech Products, Inc., Rancho Dominguez, CA) prior to lithography. All samples were cleaned in acetone and isopropanol with ultrasonic agitation in preparation for processing. The general bulk titanium process flow included the following steps: (1) TiO<sub>2</sub> mask deposition; (2) photolithographic patterning; (3) mask oxide etching; and (4) titanium deep etching. The oxide etch and titanium deep etch were both performed using the same ICP etch tool (Panasonic E640-ICP dry etching system, Panasonic Factory Solutions, Osaka, Japan), which is shown schematically in Fig. 1. The titanium samples were mounted on a 6-in. silicon carrier wafer using diffusion pump fluid (Santovac 5, polyphenyl ether pump fluid, Santovac Fluids, Inc., St. Charles, MO), which was used to create adequate thermal conductivity between carrier wafer and sample. The lower electrode of the etching tool was held constant at 20°C, and helium backside cooling at 400 Pa was used to maintain constant carrier wafer temperature during all etches.

The TiO<sub>2</sub> etch mask was deposited using reactive sputtering (Endeavor 3000 cluster sputter tool, Sputtered Films, Santa Barbara, CA) with a titanium target in an O<sub>2</sub>/Ar environment using the following process conditions: 10 sccm O<sub>2</sub>, 20 sccm Ar, and 2300 W power. The process pressure was approximately 5.2 mT. Each sample was sputtered for 4500 s, resulting in an average film thickness of 1.25 μm. Features were then patterned onto the TiO<sub>2</sub> mask using 3 μm thick photoresist (SPR 220-3.0, Shipley, Marlborough, MA).

The photoresist pattern was transferred into the oxide using a CHF<sub>3</sub> chemistry under the following conditions: 500 W ICP source power (13.56 MHz), 400 W sample rf power (13.56 MHz), 1 Pa pressure, and 40 sccm CHF<sub>3</sub>. Each sample was etched for 10 min, removed from the carrier wafer, and then cleaned in acetone and isopropanol with ultrasonic agitation. The remaining fluorinated

\* Electrochemical Society Student Member.

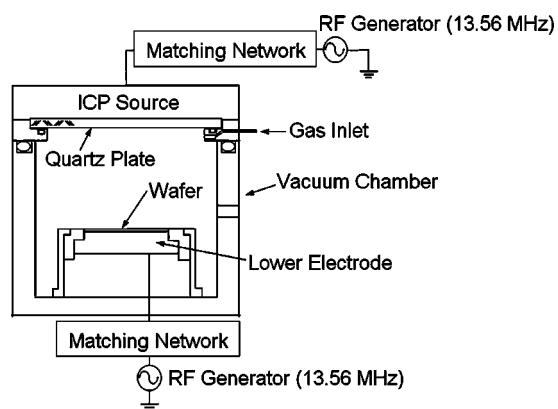


**Figure 1.** Design schematic of the Panasonic E640-ICP dry etching system. A quartz plate with an ICP source is located above an aluminum vacuum chamber facing a 6-in. carrier wafer. Two rf power sources (13.56 MHz) are applied to the ICP source and the lower electrode through a matching network. The sample carrier wafer is held to the lower electrode by an electrostatic chuck. Temperature is controlled through a helium cooling system applied to the backside of the carrier wafer. (Diagram courtesy of Panasonic Factory Solutions.)

photoresist was removed using an  $O_2$  plasma (PEII-A Plasma System, Technics) under the following conditions: 300 mT pressure, 100 W power. After cleaning, the patterned sample was remounted onto a silicon carrier wafer for the titanium deep etch. For the characterization etches, each sample was etched in a  $Cl_2/Ar$  chemistry for 2 min with a specified parameter set. Only a single parameter was varied for each etch. Unless otherwise stated, all other parameters were held constant at the following values: 400 W ICP source power (13.56 MHz), 100 W sample rf power (13.56 MHz), 2 Pa pressure, 100 sccm  $Cl_2$ , and 5 sccm Ar. Etch depths ranged from approximately 0.5 to 4.7  $\mu m$  over the chosen parameter space. The high aspect ratio etching and titanium thin-foil etching were both performed using longer etch times at parameters within the tested characterization space.

For the characterization samples, etch depth and mask thicknesses were measured using a high-resolution scanning electron microscope (FEI XL40 Sirion FEG digital scanning microscope, FEI, Hillsboro, OR). Measurements were taken on 1.5  $\mu m$  wide lines imaged at a 45° tilt angle at five random locations across the sample and averaged. These values were then compared to measurements taken using a contact stylus profilometer (Dektak IIA profilometer, Sloan) to ensure consistency. Average surface roughness measurements were also taken using an optical profilometer (Wyko NT 1100, Veeco Instruments, Inc., Woodbury, NY). Measurements were made over a large exposed area (approximately 400  $\times$  600  $\mu m$ ) at five random locations across the sample and averaged. These measurements showed as-received surface roughness levels of between 5 and 10 nm rms for the thick polished substrates. Titanium etch rate,  $TiO_2$  etch rate, and surface roughness data were plotted to determine first-order trends for each etch parameter. These trends were then used to develop the TIDE process. The high aspect ratio etching and thin-foil etching of bulk titanium followed the same general process flow used by the etch characterization runs.

### Results and Discussion

**ICP source power.**— Plasma-assisted dry etching is a combination of both physical etching through ion bombardment and chemical etching through reactive species interactions at the substrate surface.<sup>12</sup> Complete decoupling of these two etching mechanisms is difficult and the relative contributions of each can vary significantly with etch conditions. Throughout the dry etching process, the substrate surface is subjected to an incident flux of ions, radicals, electrons, and neutrals. In general, the physical processes are controlled

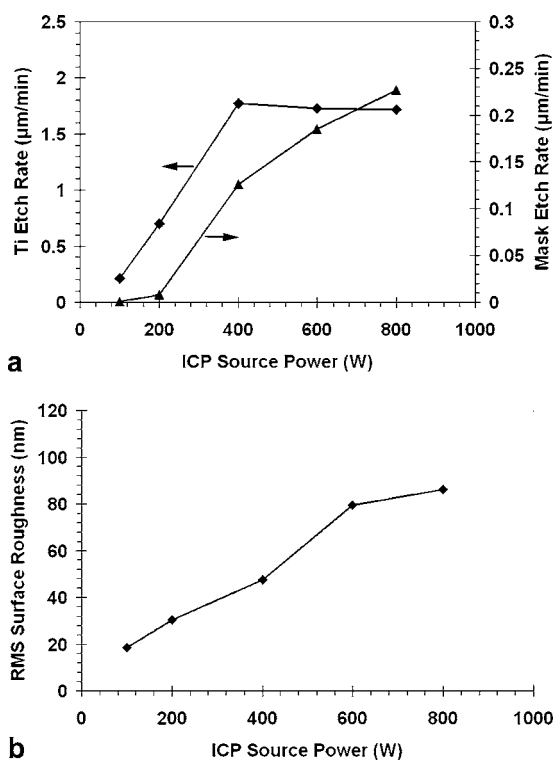


**Figure 2.** Plots showing (a) the bulk titanium and  $TiO_2$  mask etch rates and (b) the rms surface roughness as a function of ICP source power. The remaining processing parameters were held constant at 100 W rf sample power, 2 Pa, 100 sccm  $Cl_2$ , and 5 sccm Ar. Samples were etched for 2 min.

by the ion flux and the chemical processes are controlled by both the ion and radical flux.<sup>13</sup> It has been reported that titanium etching relies more heavily on chemical processes, while  $TiO_2$  etching is more dependent on physical etching.<sup>8</sup> Consequently, titanium etching will most likely be driven by chemical mechanisms and reactive species availability, whereas  $TiO_2$  etching will be affected more by ion bombardment.

The bulk titanium etch rate as a function of ICP source power is shown in Fig. 2a. Etch rate increases appreciably with source power initially and then levels off for powers above 400 W. Assuming that the chlorine-based etching mechanism associated with the etching of bulk titanium is chemically similar to that of titanium thin-film etching discussed in the literature, titanium tetrachloride  $TiCl_4$  is the most volatile etch compound with a boiling temperature of 136.4°C.<sup>4,6</sup> However, both  $TiCl_4$  and  $TiCl_2$  (boiling temperature = 1327°C) have been detected as reaction products.<sup>6,14</sup> As molecular  $Cl_2$  is introduced into the discharge, a percentage will be ionized or dissociated into atomic Cl. Increased source power will lead to an increase in this ionization and dissociation, resulting in higher ion and radical densities.<sup>7</sup> Below 400 W, the etching of bulk titanium is most likely ion and radical limited, resulting in a decrease in overall chemical reaction and etch rate. As the reactive species density is increased with increasing power, the etch rate will also increase. For values above 400 W, the ionization and dissociation of chlorine is no longer the limiting factor. In this range the etch rate is most likely controlled by other processes, such as the supply rate of the reactive chlorine species, the reactive species transport rate to the substrate surface, or the chemical reaction rate at the surface. This causes the etch rate to remain constant for values above 400 W if all other parameters are held constant.

ICP source power also influences the quality of the etched feature surface. As shown in Fig. 3, source power affects both the roughness and overall shape of the etched features. For lower source power, i.e., 200 W, the resultant etch appears to be more isotropic, leading

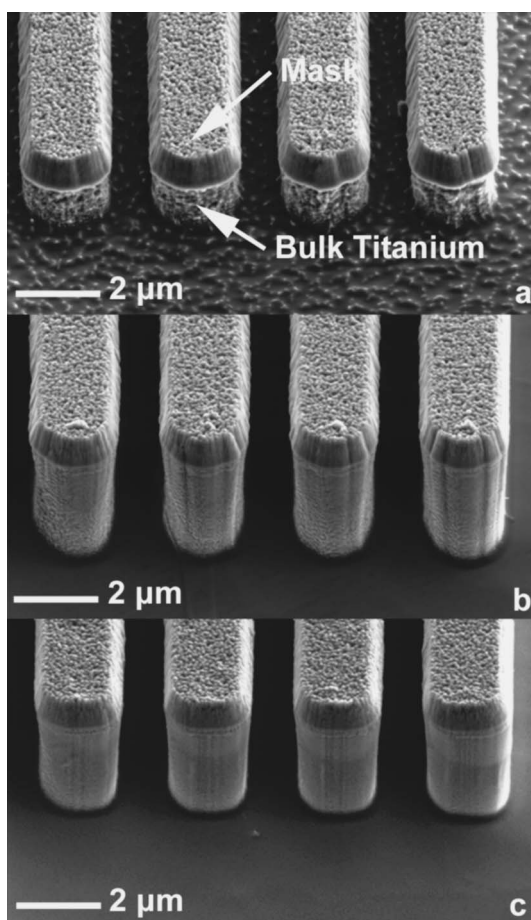


**Figure 3.** Scanning electron micrographs, taken at a 45° tilt, showing features etched at various ICP source powers: (a) 200 W; (b) 400 W; and (c) 600 W. The remaining processing parameters were held constant at 100 W rf sample power, 2 Pa, 100 sccm Cl<sub>2</sub>, and 5 sccm Ar. Samples were etched for 2 min.

to a slight undercutting of the TiO<sub>2</sub> masking layer. This lower power also results in microscopic roughness on all exposed titanium surfaces, attributed to a higher chemical etch component. As source power is increased to 400 W incident ion flux increases, which results in reduced sidewall and floor roughness. Increasing the source power to 600 W does not increase etch rate considerably; however, it does further reduce sidewall and floor roughness. Higher ICP source power may also improve the verticality of the etch; however, this is a difficult conclusion to make from low aspect ratio features such as those shown in Fig. 3.

The TiO<sub>2</sub> etch rate as a function of ICP source power is also shown in Fig. 2a. The etch rate increases only slightly between 100 and 200 W but then increases drastically for values above 200 W. This results in a decrease in overall TiO<sub>2</sub> mask selectivity. At lower powers, the ion concentrations and energies are lower, thereby reducing ion bombardment. As the source power is increased the incident ion flux increases, which will in turn increase the TiO<sub>2</sub> etch rate. Therefore, a trade-off exists between increasing the titanium etch rate and maintaining high TiO<sub>2</sub> mask selectivity through manipulation of ICP source power.

Optical profilometry was used to study resulting surface roughness following each characterization etch. This method allowed for the measurement of large surface areas (400 × 600 μm) comparable to typical MEMS device dimensions. Root-mean-square (rms) surface roughness as a function of ICP source power is shown in Fig. 2b. The rms surface roughness ( $R_{\text{rms}}$ ) increases with increasing ICP source power. This increase can be attributed to roughening at

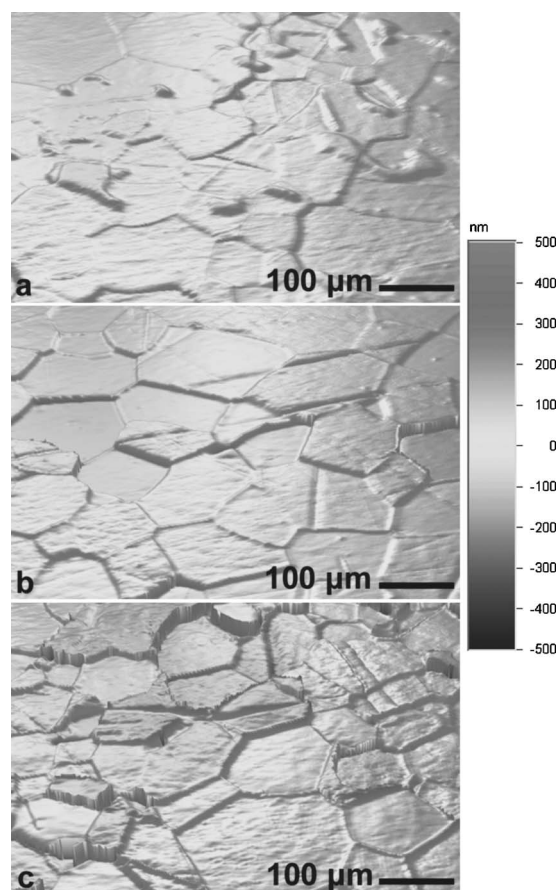


**Figure 4.** Three-dimensional surface profiles measured using phase-shift interferometry of bulk titanium following a 2 min etch at various ICP source powers: (a) 200 W; (b) 400 W; and (c) 600 W. The remaining processing parameters were held constant at 100 W rf sample power, 2 Pa, 100 sccm Cl<sub>2</sub>, and 5 sccm Ar. The measured region is approximately 400 × 600 μm.

both the global and local scales, as shown in Fig. 4. The thick titanium substrates used for the etch characterization are polycrystalline in nature,<sup>15</sup> with grain sizes on the order of ~100 μm. Differential etching of these grains, presumably due to preferential etching of certain crystallographic orientations, increases roughness on the global scale. As the ICP source power is increased from 200 to 400 W, the variation in etch depth between various grains is increased, leading to an overall increase in  $R_{\text{rms}}$ . As the ICP source power is further increased to 600 W, additional features can be seen along the grain boundaries. These features were often found to cause micromasking during longer etches, and may be caused by the localization of impurities during the titanium sheet production process.<sup>15</sup>

Though the aforementioned global roughness due to grain structure and boundaries will more strongly effect the quality of a typical titanium MEMS device, local roughness can also be assessed qualitatively using the same measurements. For example, increasing ICP source power is also observed to cause a slight increase of local roughness within the grains themselves. This local roughness is at a smaller length scale than the aforementioned global roughness, but should not be confused with the microscopic roughness seen in Fig. 3a, which is most likely below the discernible length scale for the tool and experimental setup being used. An increase in local roughness was made more apparent with the application of a high-pass digital filter using a fast Fourier transform (FFT) to filter surface roughness data with spatial frequency below 10 μm. Application of this filtering to the roughness measurements of the surfaces shown in Fig. 4 at 400 and 600 W ICP source power yielded  $R_{\text{rms}}$  values of

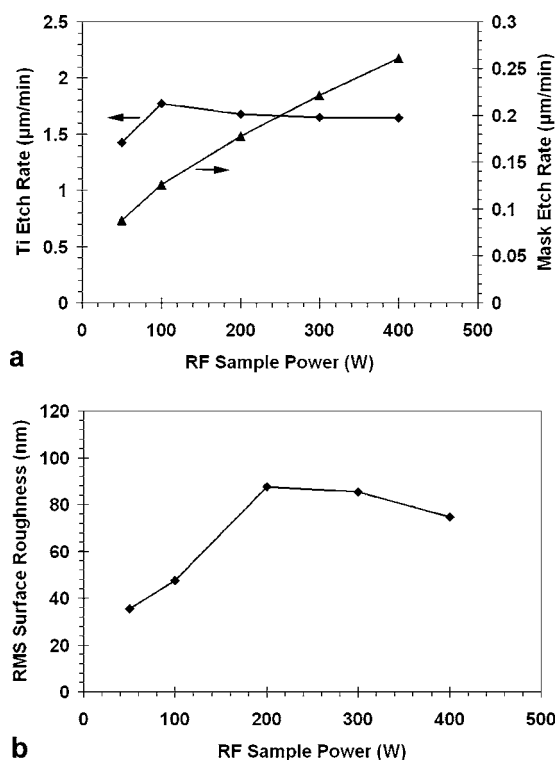


**Figure 5.** Plots showing (a) the bulk titanium and  $\text{TiO}_2$  mask etch rates and (b) the rms surface roughness as a function of rf sample power. The remaining processing parameters were held constant at 400 W ICP source power, 2 Pa, 100 sccm  $\text{Cl}_2$ , and 5 sccm Ar. Samples were etched for 2 min.

roughly 5 and 10 nm, respectively. This suggests that the average local roughness at 600 W ICP is twice that at 400 W. Similarly, if the FFT filter is applied to the roughness measurement for an etch with 800 W ICP source power, the resultant rms value is  $\sim 25$  nm, 5 times higher than the value at 400 W. The data filtering therefore confirms that increased ICP source power produces increased local roughness, as the surface profiles in Fig. 4 suggest. This, in combination with an increase in global roughness, most likely contributes to the increase in overall surface roughness associated with higher ICP source powers.

**RF sample power.**—The applied rf sample power, or bias, controls the incident ion energy on the surface of the substrate.<sup>12</sup> Figure 5a shows the bulk titanium etch rate as a function of rf sample power. The titanium etch rate increases slightly with increasing bias from 50 to 100 W, but then remains relatively constant for values above 100 W. As mentioned previously, it has been reported that titanium etching is more dependent on chemical processes than ion bombardment.<sup>8</sup> However, it is likely energetic ions will partially assist the removal of material from the substrate surface. Therefore, for bias values below 100 W, the level of incident ion energy may limit the titanium etch rate. For values above 100 W, ion bombardment is no longer the limiting factor and the titanium etch rate is most likely dependent on other factors controlling chemical processes within the plasma. This causes the etch rate to remain constant for bias values above 100 W if all other parameters are held constant.

When compared to variations in ICP source power, rf sample bias has much less effect on the titanium etch rate for the tested values. Varying the sample bias only resulted in changes in etch rate in the range of 0.5  $\mu\text{m}/\text{min}$ . However, similar to ICP source power, variations in rf sample power did strongly influence the microscopic roughness of the exposed titanium surfaces. As shown in Fig. 6, as sample bias is increased from 50 to 200 W the resultant etch ap-

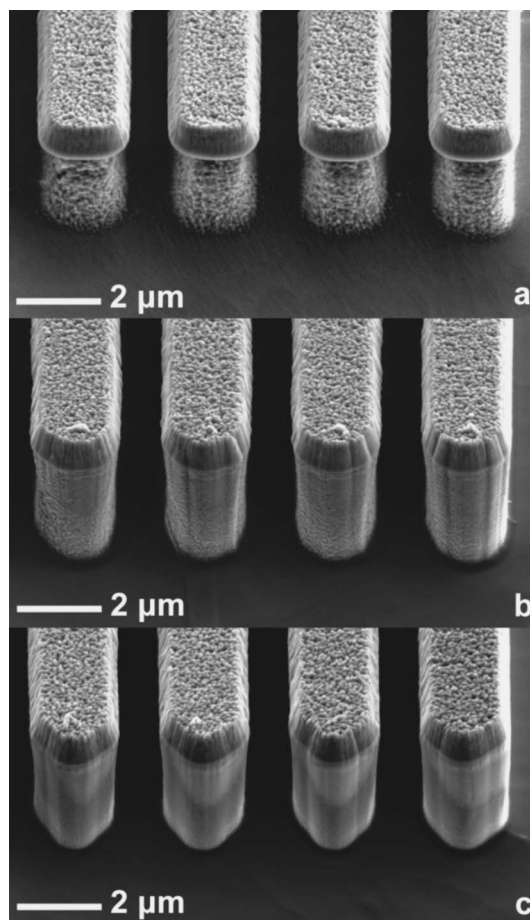


**Figure 6.** Scanning electron micrographs, taken at a 45° tilt, showing features etched at various rf sample powers: (a) 50 W; (b) 100 W; and (c) 200 W. The remaining processing parameters were held constant at 400 W ICP source power, 2 Pa, 100 sccm  $\text{Cl}_2$ , and 5 sccm Ar. Samples were etched for 2 min.

pears to become more anisotropic. In particular, the sidewalls associated with sample bias 50 W are extremely rough and show under-cutting of the  $\text{TiO}_2$  mask. However, unlike the etched features associated with lower ICP source powers (refer to Fig. 3a), the resulting feature roughness at this low sample bias is very apparent on the sidewalls but does not appear on the etched floors. Therefore, the etch appears to be less chemical and more directional at this low sample bias than in the case of low ICP source power, i.e., 200 W, where the entire surface showed microscopic roughness. As sample bias is increased to 200 W virtually all roughness on the sidewalls is removed and the resulting features are smooth. And, there may also be some improvement in the verticality of the etched features though, again, this is difficult to conclude from low aspect ratio features such as those shown in Fig. 6.

Variations in rf sample power were found to have only a small effect on the titanium etch rate. However, rf sample power did strongly affect the  $\text{TiO}_2$  mask selectivity. As sample bias is increased from 50 to 400 W, the  $\text{TiO}_2$  mask etch rate almost triples, as shown in Fig. 5a. This is most likely due to the increase in ion bombardment energy associated with higher rf sample powers. Therefore, increasing sample bias will improve etch anisotropy but reduce overall  $\text{TiO}_2$  mask selectivity.

The surface roughness,  $R_{\text{rms}}$ , as a function of rf sample power is shown in Fig. 5b. Surface roughness increases significantly as bias increases from 50 to 200 W. Above 200 W,  $R_{\text{rms}}$  tends to decrease slightly. An analysis was performed similar to that done for ICP source powers for bias values of 200 and 400 W to determine the

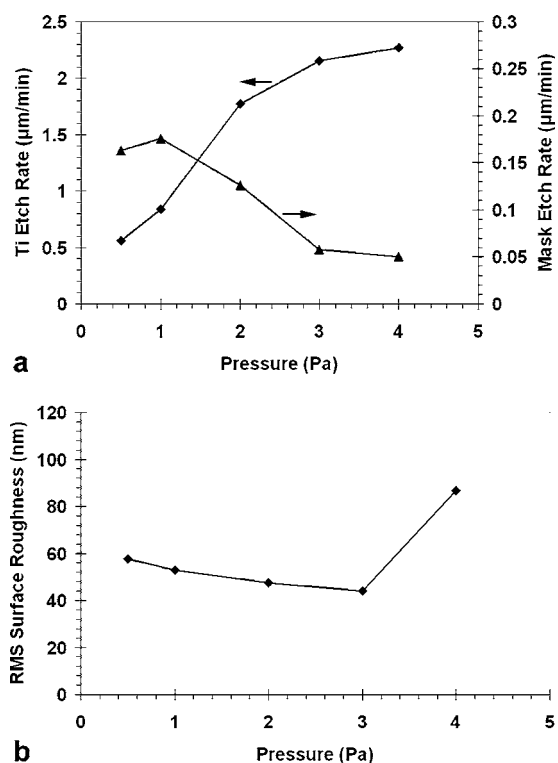


**Figure 7.** Plots showing (a) the bulk titanium and TiO<sub>2</sub> mask etch rates and (b) the rms surface roughness as a function of chamber pressure. The remaining processing parameters were held constant at 400 W ICP source power, 100 W rf sample power, 100 sccm Cl<sub>2</sub>, and 5 sccm Ar. Samples were etched for 2 min.

nature of this decrease in overall surface roughness. The raw data suggest that global surface roughness attributed to grain orientation and boundaries is more pronounced for a 200 W bias when compared to a 400 W bias (not shown). When a high-pass FFT filter was applied to remove data with spatial frequencies below 10 μm, the local surface roughness between the two bias values appeared roughly comparable. Therefore, increasing bias above 200 W does not seem to further increase local roughness on the grain surfaces, even though higher ion bombardment is attributed to higher bias. Instead, the higher bias appears to slightly reduce large-scale roughness associated with grain boundaries, in effect smoothing the surface.

**Pressure.**—Figure 7a shows the bulk titanium etch rate as a function of pressure. The etch rate is strongly influenced by pressure, increasing significantly from 0.5 to 4.0 Pa. As pressure is increased, less directional etching associated with an increase in randomized collisions between particles will occur.<sup>16</sup> In this regime, chemical effects are dominant<sup>12</sup> and directional ion bombardment will be reduced. This may lead to an increase in titanium etch rate. The dominance of these chemical effects is better visualized in Fig. 8. As the pressure is increased from 1 to 2 Pa, the images show both an increase in etch rate and an increase in sidewall microscopic roughness. As the pressure is further increased to 3 Pa, roughness increases on the sidewalls of the etched features as well as the floor of the substrate. At 3 Pa, there also appears to be a significant degree of mask undercutting associated with more isotropic etch behavior. The isotropic nature of the etch in this pressure range is most likely due to the predicted dominance of chemical processes.

The TiO<sub>2</sub> mask etch rate as a function of chamber pressure is also shown in Fig. 7a. The etch rate shows a slight increase between 0.5 and 1 Pa and then proceeds to decrease between 1 and 4 Pa. Above 1 Pa, the ion bombardment may be reduced due to an in-

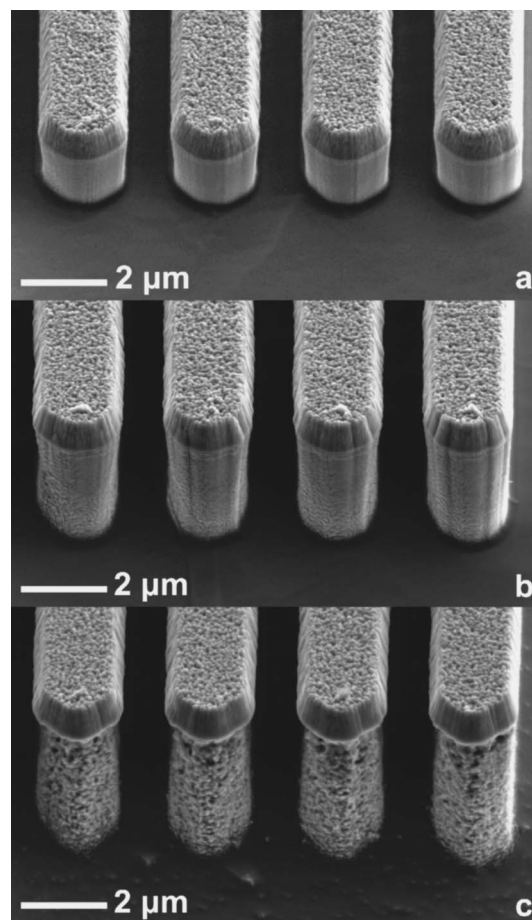


**Figure 8.** Scanning electron micrographs, taken at a 45° tilt, showing features etched at various chamber pressures: (a) 1 Pa; (b) 2 Pa; and (c) 3 Pa. The remaining processing parameters were held constant at 400 W ICP source power, 100 W rf sample power, 100 sccm Cl<sub>2</sub>, and 5 sccm Ar. Samples were etched for 2 min.

crease in the number of random particle collisions. This results in a decrease in the overall TiO<sub>2</sub> etch rate leading to increased selectivity. The TiO<sub>2</sub> selectivity changes from roughly 3:1 for a process pressure of 1 Pa to 45:1 at 4 Pa. Therefore, pressure was found to have the second largest effect on selectivity after ICP source power. However, higher pressure will also result in a more isotropic etch profile, as shown in Fig. 8. Therefore, a trade-off between mask selectivity and etch anisotropy must be taken into consideration when determining optimal process pressure for the deep etching of high aspect ratio features.

The surface roughness,  $R_{\text{rms}}$ , as a function of chamber pressure is shown in Fig. 7b. Surface roughness decreases slightly from 0.5 to 3 Pa and then increases significantly for a chamber pressure of 4 Pa. Figure 9 shows sample surface profiles for chamber pressure values of 2, 3, and 4 Pa. At 2 Pa, the surface shows nominal grain structure and local roughness. As pressure is increased to 3 Pa, global roughness due to grain boundaries and preferential grain etching seems to decrease slightly and local roughness on the grain surfaces seems to increase. At 4 Pa, grain structure definition is further diminished and overall local roughness is very apparent. This overall increase in local roughness, as well as some associated grain boundary features visible in the surface profile, most likely leads to the large increase in overall  $R_{\text{rms}}$  values at this pressure. This local roughness was further quantified using the previously described filtering technique to remove roughness with spatial frequencies below 10 μm. When the raw surface data are compared for the pressures 2 and 4 Pa, some increase in global roughness associated with the

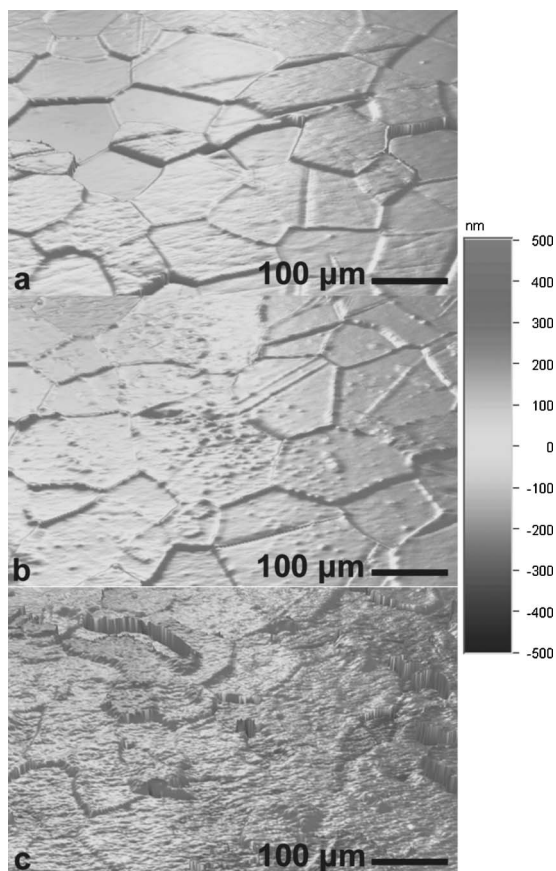


**Figure 9.** Three-dimensional surface profiles measured using phase-shift interferometry of bulk titanium following a 2 min etch at various chamber pressures: (a) 1 Pa; (b) 2 Pa; and (c) 3 Pa. The remaining processing parameters were held constant at 400 W ICP source power, 100 W rf sample power, 100 sccm  $\text{Cl}_2$ , and 5 sccm Ar. The measured region is approximately  $400 \times 600 \mu\text{m}^2$ .

grain boundaries is noted at the higher pressure. However, when the data are filtered the difference in overall, local roughness is significant. Specifically, the filtered, local roughness  $R_{\text{rms}}$  value increases from roughly 5 nm at 2 Pa to 25 nm at 4 Pa. Therefore, the local roughness component of the overall  $R_{\text{rms}}$  is most likely the major cause of the surface roughness increase at 4 Pa.

**Gas composition.**—Figure 10a shows the bulk titanium etch rate as a function of  $\text{Cl}_2$  gas flow rate. The etch rate increases from roughly 0.8 to 1.8  $\mu\text{m}/\text{min}$  as the  $\text{Cl}_2$  flow rate is increased from 20 to 40 sccm. From 40 to 100 sccm, the etch rate remains relatively constant, increasing only slightly with increasing  $\text{Cl}_2$  flow rate. The availability of the reactant species within the plasma is determined by the rate of introduction to the discharge vs the rate of chemical reaction with the substrate.<sup>7</sup> The chlorine reactant species will be introduced to the plasma through atomic dissociation and ionization of the incoming gas flow. Higher gas flow rates result in shorter molecular residence times within the plasma, which will, in turn, reduce the percentage of dissociation of the incoming gas.<sup>17</sup> The increase in etch rate between 20 and 40 sccm might reflect limitations in reactant species availability as it is lost to chemical reactions at the titanium surface. Above this value, the plasma remains saturated with the reactant species. The etch rate in this range of  $\text{Cl}_2$  flow rate remains relatively constant and may be limited instead by the reaction rate at the titanium surface or by the rate of molecular dissociation. Higher flow rates also result in slightly rougher feature sidewalls, as shown in Fig. 11. This figure also illustrates the increase in etch rate as the  $\text{Cl}_2$  flow rate is increased

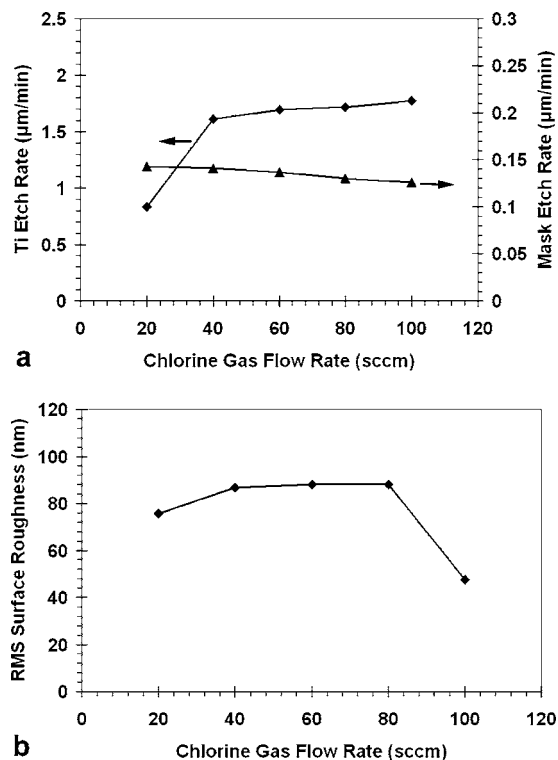


**Figure 10.** Plots showing (a) the bulk titanium and  $\text{TiO}_2$  mask etch rates and (b) the rms surface roughness as a function of chlorine gas flow rate. The remaining processing parameters were held constant at 400 W ICP source power, 100 W rf sample power, 2 Pa, and 5 sccm Ar. Samples were etched for 2 min.

from 20 to 60 sccm. However, at both of these flow rates the side-walls of the etched features remain smooth. As the  $\text{Cl}_2$  flow rate is further increased to 100 sccm, there is little change in etch rate when compared to 60 sccm. However, microscopic sidewall roughness begins to appear at the base of the etched features. Figure 10a also shows the  $\text{TiO}_2$  mask etch rate as a function of  $\text{Cl}_2$  gas flow rate. The etch rate remains relatively constant at all flow rates, decreasing only slightly from 20 to 100 sccm. Therefore,  $\text{Cl}_2$  flow rate seems to have little to no effect on mask selectivity.

Figure 12a shows the bulk titanium etch rate as a function of increasing Ar gas flow rate, holding the  $\text{Cl}_2$  flow rate constant at 100 sccm. The etch rate increases slightly with the introduction of Ar to the plasma, but then remains relatively constant at increasing Ar flow rates. The addition of an inert gas to a discharge is often used to stabilize the plasma or to control etchant concentration without varying pressure.<sup>7</sup> The addition of Ar to a chlorine plasma has been reported to increase etch rate under constant pressure for various materials.<sup>18</sup> Several mechanisms may be responsible for this behavior, including increased  $\text{Cl}_2$  dissociation through interactions with metastable Ar atoms or increased surface bombardment by energetically active species.<sup>18,19</sup> Although a slight increase in titanium etch rate is seen with the addition of a small amount of Ar, the relative change is not significant.

Gas composition partial pressures were also manipulated in order to more broadly understand the effects of Ar addition on the  $\text{Cl}_2$ -based etching of bulk titanium. Figure 12b shows the bulk titanium etch rate as a function of percentage Ar, maintaining the total flow rate at 100 sccm. Initially the etch rate remains constant as Ar content is increased to 10% and  $\text{Cl}_2$  content is decreased to 90%. As the Ar is further increased to 50% partial pressure, the etch rate decreases, most likely due to the decrease in overall  $\text{Cl}_2$  partial pressure affecting reactive species availability. Therefore, the addition of a small amount of Ar to a  $\text{Cl}_2$ -based plasma seems to increase

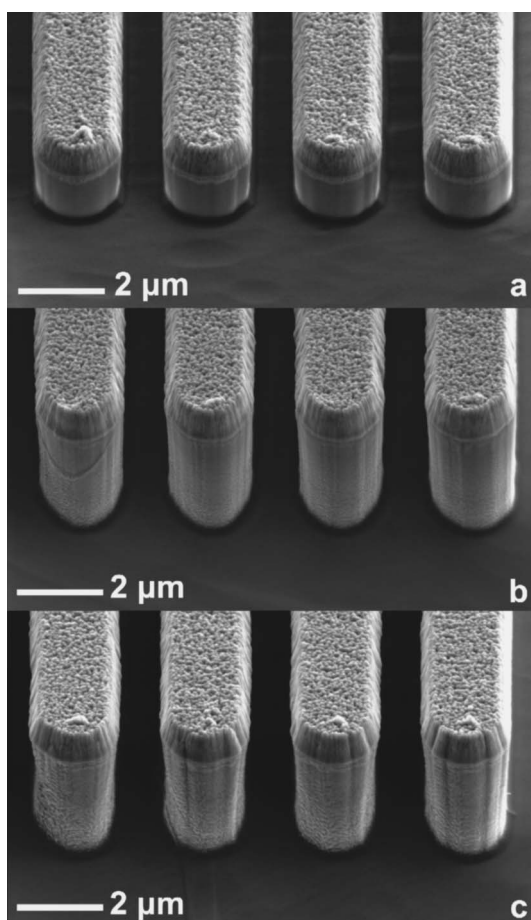


**Figure 11.** Scanning electron micrographs, taken at a 45° tilt, showing features etched at various chlorine gas flow rates: (a) 20 sccm; (b) 60 sccm; and (c) 100 sccm. The remaining processing parameters were held constant at 400 W ICP source power, 100 W rf sample power, 2 Pa, and 5 sccm Ar. Samples were etched for 2 min.

the overall bulk titanium etch rate. However, further increasing the Ar content does not appear to promote higher etch rates beyond this initial increase. The TiO<sub>2</sub> etch rate as a function of percentage Ar composition is also shown in Fig. 12b. The etch rate decreases initially as Cl<sub>2</sub> content is dropped to 90% and Ar content is increased to 10%. Above 10% Ar, the etch rate increases. This initial decrease in etch rate is not well understood at this time. However, the increasing TiO<sub>2</sub> etch rate at higher Ar partial pressures is most likely due to higher ion bombardment.

As mentioned earlier, if the Ar flow rate into the plasma is increased to 5 sccm while holding the Cl<sub>2</sub> flow rate constant at 100 sccm, a slight increase in etch rate is realized. In addition, if the Ar flow rate is further increased, the etch rate remains relatively constant. However, the quality of the etched features will change with higher Ar content, as shown in Fig. 13. At 5 sccm Ar flow rate, the sidewalls show some roughening at the base of the etched features. As the Ar is increased to 10 sccm, this roughness covers the entire exposed sidewall surface and a slight undercutting of the TiO<sub>2</sub> mask occurs.

The root-mean-square surface roughness was also measured for both Cl<sub>2</sub> gas flow rate and Ar composition. Figure 10b shows that for Cl<sub>2</sub> gas flow rate the  $R_{rms}$  increases slightly from 20 to 40 sccm, and then remains somewhat constant from 40 to 80 sccm. The surface roughness then drops significantly from 80 to 100 sccm. Higher  $R_{rms}$  values at lower Cl<sub>2</sub> flow rates may be due in part to an increase in overall Ar partial pressure at lower Cl<sub>2</sub> flow rates as the pressure is held constant. Higher Ar percentage will lead to higher

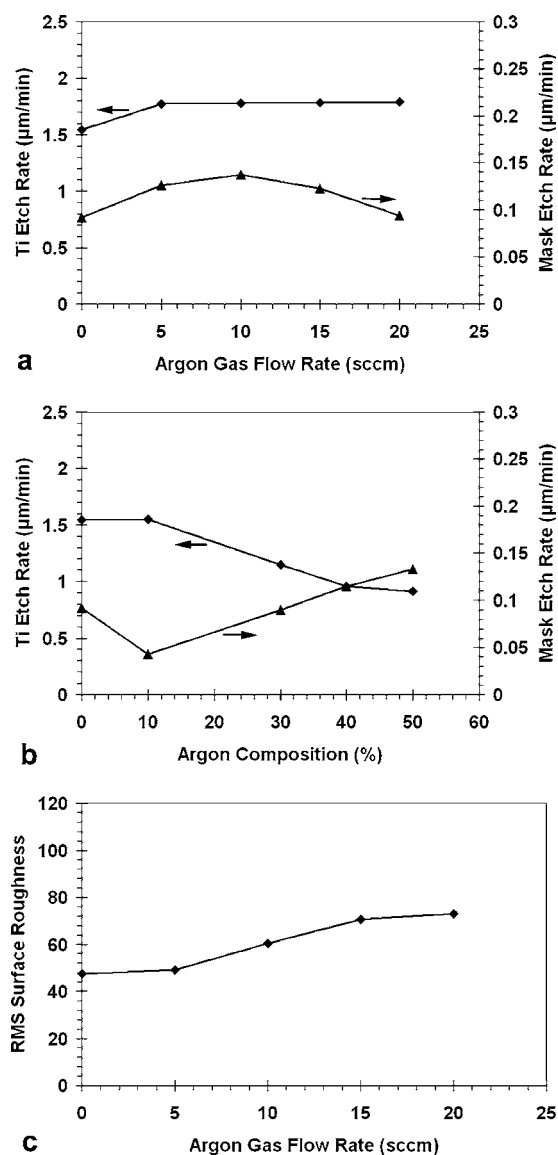


**Figure 12.** Plots showing (a) the bulk titanium and TiO<sub>2</sub> mask etch rates as a function of argon gas flow rate; the chlorine gas flow rate was held constant at 100 sccm; (b) the bulk titanium and TiO<sub>2</sub> mask etch rate as a function of argon composition; the overall gas flow rate was held constant at 100 sccm, and (c) the rms surface roughness as a function of argon gas flow rate. The remaining processing parameters were held constant at 400 W ICP source power, 100 W rf sample power, and 2 Pa. Samples were etched for 2 min.

ion bombardment, thus increasing the overall surface roughness. At 100 sccm, the etch becomes slightly more chemical, as discussed above, and the relative Ar partial pressure is small. This may lead to the drop in  $R_{rms}$  values seen at 100 sccm. Similar  $R_{rms}$  measurements have been made for Ar gas flow rate, as shown in Fig. 12c. As the Ar gas flow rate is increased from 0 to 20 sccm, holding the Cl<sub>2</sub> flow rate constant at 100 sccm, the surface roughness increases steadily. Again, this is most likely due to increasing ion bombardment associated with higher Ar flow rates.

**Application to MEMS.**—Based on the results of the etch characterization described above, initial baseline process conditions were selected for etches which resulted in greater etch depths and aspect ratios. Such features are a fundamental characteristic of many bulk micromachined MEMS devices, especially those that rely on structures with vertical sidewalls and precisely defined gaps for electrostatic actuation and sensing. Figure 14 shows a typical

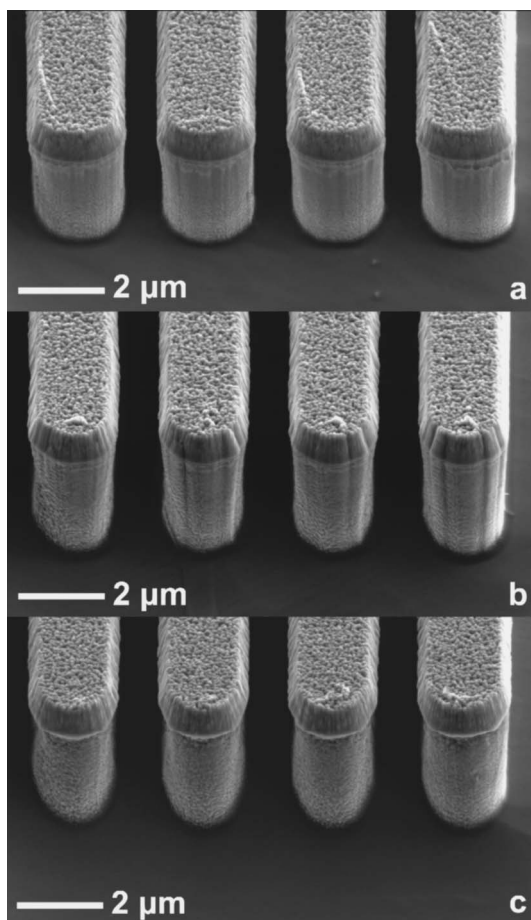


**Figure 13.** Scanning electron micrographs, taken at a 45° tilt, showing features etched at various argon gas flow rates: (a) 0 sccm; (b) 5 sccm; and (c) 10 sccm. The remaining processing parameters were held constant at 400 W ICP source power, 100 W rf sample power, 2 Pa, and 100 sccm Cl<sub>2</sub>. Samples were etched for 2 min.

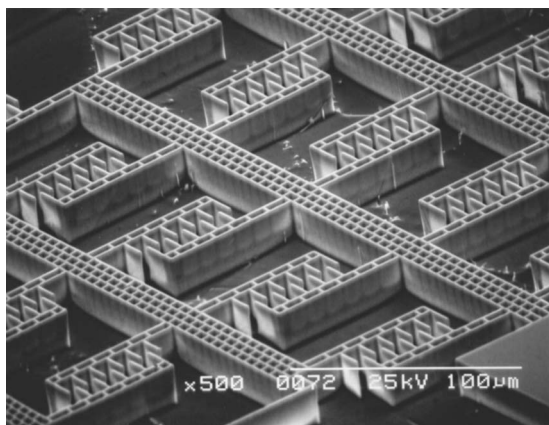


**Figure 14.** Scanning electron micrograph of a titanium-based MEMS comb drive structure. The mask pattern was generated using optical lithography, transferred to a sputtered TiO<sub>2</sub> mask via a CHF<sub>3</sub>-based dry etch, then the sample was deep etched for 10 min using the TIDE process (400 W ICP source power, 100 W sample rf power, 2 Pa pressure, 100 sccm Cl<sub>2</sub>, and 5 sccm Ar). Etch depth in the open areas of the pattern is slightly in excess of 20 μm. The reduction of etch rate within the narrow vias can be seen through the thin sidewalls of the backbone structures and is indicative of RIE lag.

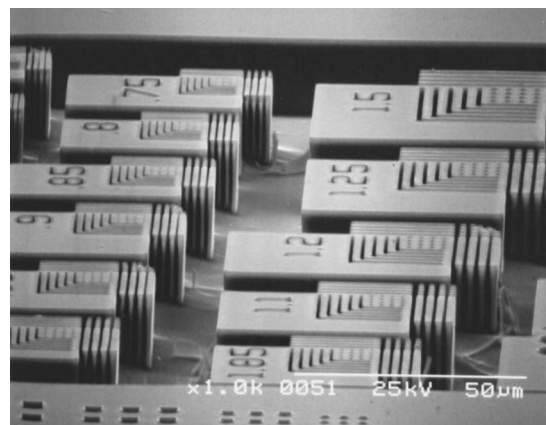


**Figure 15.** Scanning electron micrograph illustrating sub-micrometer minimum feature size capability. Etched numerals indicate feature size in micrometers. This sample was etched for 7 min using the baseline TIDE process (400 W ICP source power, 100 W sample rf power, 2 Pa pressure, 100 sccm Cl<sub>2</sub>, and 5 sccm Ar).

MEMS comb drive structure with a minimum feature size of 1 μm etched into a thick titanium substrate using these initial baseline process parameters (400 W ICP source power, 100 W sample rf power, 2 Pa pressure, 100 sccm Cl<sub>2</sub>, and 5 sccm Ar). As can be seen, these conditions enable the definition of high aspect ratio structures with smooth, vertical sidewalls and well-controlled gaps. However, aspect-ratio-dependent-etching (ARDE) phenomena not observed in the previous etch characterization study also began to emerge. For example, as can be seen in Fig. 14, narrow cavities within the comb drive structure are etched more slowly than the surrounding open features. This can be attributed to RIE lag, and is associated with local transport phenomena.<sup>20-22</sup> Such effects were not observed in the previous etch characterization studies due to the short etch times used (2 min), which produced features with relatively low aspect ratios (maximum 3:1). Figure 15 shows the base-

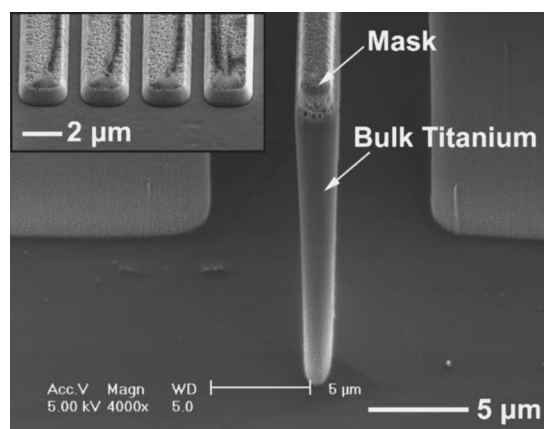


**Figure 16.** Scanning electron micrographs of the TiO<sub>2</sub> mask following the CHF<sub>3</sub> etch and solvent cleaning, prior to O<sub>2</sub> plasma to strip remaining fluorinated photoresist (inset) and a deep etched feature using a similarly defined mask. The sidewalls and floor of the etched feature appear relatively smooth except toward the top, where the periphery of the mask was lost during the etch process. The CHF<sub>3</sub> etch currently being used to transfer patterns into the TiO<sub>2</sub> masking layer results in slightly sloped sidewalls. This sloping causes loss of mask which transfers into the deep etched titanium as the etch progresses. This sample was etched for 10 min using the baseline TIDE process with increased sample rf power (150 vs 100 W) and pressure (2.5 vs 2 Pa).

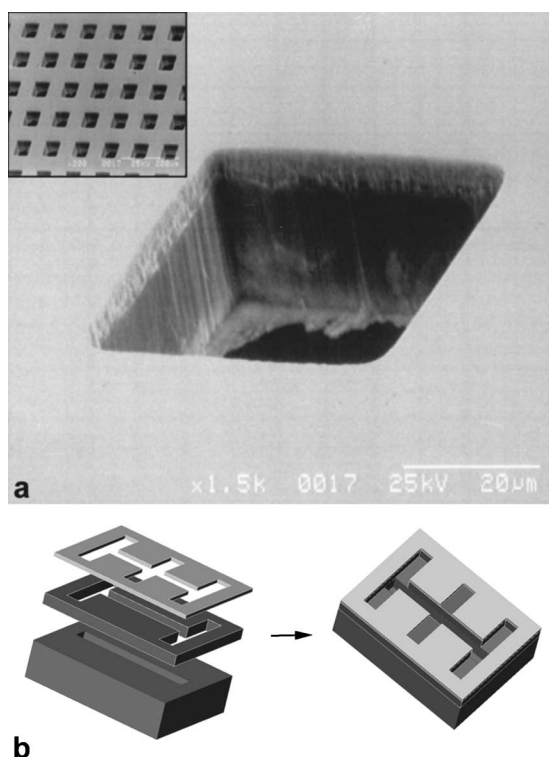


**Figure 17.** (a) Scanning electron micrograph of a through-etched titanium thin foil showing an array of  $50 \times 50 \mu\text{m}$  square features (inset) and a closer look at a single square. The titanium foil was  $25 \mu\text{m}$  thick and required 12 min to through-etch using the standard TIDE process. The floors of the feature are not completely cleared but additional etching should remove any remaining titanium. (b) A schematic depicting the concept of stacking and bonding through-etched thin titanium foils in order to create complex three-dimensional structures of arbitrary cross section.

line TIDE process is also capable of etching sub-micrometer features.

Variation of process conditions about the initial baseline conditions described above resulted in the development of a more optimized TIDE parameter set, which entailed increased rf sample power and chamber pressure (400 W ICP source power, 150 W rf sample power, 2.5 Pa, 100 sccm  $\text{Cl}_2$ , and 5 sccm Ar). These conditions were then used to etch the high aspect ratio feature shown in Fig. 16. The etch rate and selectivity for these etch conditions were approximately  $2.2 \mu\text{m}/\text{min}$  and 40:1 (Ti: $\text{TiO}_2$ ), respectively. These parameters resulted in deep etched features with good verticality (some tapering noticeable) and relatively smooth sidewalls. Slight microroughness did appear towards the base of the features. Roughness toward the top of the etched features is most likely due to loss of mask, which was found to be dependent on the quality of the oxide etch. As can be seen in Fig. 16, the  $\text{CHF}_3$  etch used to define the mask pattern results in slightly sloped sidewalls, which eventually causes loss of mask around the periphery of the feature as the etch progresses. In the future, this issue may be resolved by either improving the directionality of the  $\text{CHF}_3$  oxide etch or by using additional masking materials with even higher selectivity. One such example currently being pursued is a metal mask defined by a standard lift-off procedure with high selectivity to chlorine etchants. This would also eliminate the long sputter time associated with the current  $\text{TiO}_2$  mask. However, as with any high aspect ratio etch process, thorough optimization of the masking material and overall

TIDE process will depend strongly on the desired aspect ratios and patterns being used and, therefore, will have to be approached on an application-by-application basis.

The TIDE process can also be used to etch thin titanium foils of varying thickness (10 to  $100 \mu\text{m}$ ). This etching can be used to etch completely through a foil, as shown in Fig. 17a. Through-etched titanium foils offer a new method to design and manufacture microdevices with arbitrary 3D cross sections through successive stacking and bonding of individual foils onto a substrate.<sup>2</sup> Bonding methods may include gold-gold thermal compression or anodic bonding. This concept is shown schematically in Fig. 17b.

### Conclusion

The preliminary characterization of bulk titanium dry etching using an ICP source is reported. The ICP source power, sample rf power, process pressure, and gas composition were varied in order to determine first-order effects on the titanium etch rate, the  $\text{TiO}_2$  mask etch rate, and surface roughness associated with each parameter. Based on this etch characterization, initial results for the high aspect ratio etching of bulk titanium are presented. Using the TIDE process, bulk titanium etch rates in excess of  $2 \mu\text{m}/\text{min}$  with high mask selectivity (40:1, Ti: $\text{TiO}_2$ ) are possible under optimized conditions. The TIDE process offers a high etch rate, smooth sidewall alternative to the MARIO process for the etching of bulk titanium. The TIDE process expands titanium bulk micromachining capability and provides further potential for the realization of novel titanium-based MEMS devices.

### Acknowledgments

The authors thank Motohiko Arakawa at Tokyo Stainless Grinding, Company Limited, and Mitsuru Hiroshima at Panasonic Factory Solutions. This research was funded by the Microsystems Technology Office at the Defense Advanced Research Projects Agency.

University of California assisted in meeting the publication costs of this article.

### References

1. S. M. Spearing, *Acta Mater.*, **48**, 179 (2000).
2. M. F. Aimi, M. P. Rao, N. C. MacDonald, A. S. Zuruzi, and D. P. Bothman, *Nat. Mater.*, **3**, 103 (2004).
3. D. M. Brunette, P. Tengvall, M. Textor, and P. Thomsen, *Titanium in Medicine: Material Science, Surface Science, Engineering, Biological Responses and Medical Applications*, p. 3, Springer, Berlin (2001).
4. K. Blumenstock and D. Stephani, *J. Vac. Sci. Technol. B*, **7**, 627 (1989).
5. P. Unger, V. Bogli, and H. Beneking, *Microelectron. Eng.*, **5**, 279 (1986).
6. R. d'Agostino, F. Fracassi, and C. Pacifico, *J. Appl. Phys.*, **72**, 4351 (1992).
7. N. M. Muthukrishnan, K. Amberiadis, and A. Elshabini-Riad, *J. Electrochem. Soc.*, **144**, 1780 (1997).
8. Y. Kuo and A. G. Schrott, in *ULSI Science and Technology/1995*, E. M. Middelworth and H. Massoud, Editors, PV 95-5, p. 246, The Electrochemical Society Proceedings Series, Pennington, NJ (1995).
9. R. d'Agostino, F. Fracassi, C. Pacifico, and P. Capezzuto, *J. Appl. Phys.*, **71**, 462 (1992).
10. R. R. Reeves, M. Rutten, S. Ramaswami, and P. Roessle, *J. Electrochem. Soc.*, **137**, 3517 (1990).
11. C. O'Mahoney, M. Hill, P. J. Hughes, and W. A. Lane, *J. Micromech. Microeng.*, **12**, 438 (2002).
12. M. J. Madou, *Fundamentals of Microfabrication*, p. 78, 103, CRC Press, Boca Raton, FL (2002).
13. S. A. Campbell, *The Science and Engineering of Microelectronic Fabrication*, p. 266, 514, Oxford University Press, New York (2001).
14. W. L. O'Brien, T. N. Rhodin, and L. C. Rathbun, *J. Chem. Phys.*, **89**, 5264 (1988).
15. M. J. Donachie, *Titanium: A Technical Guide*, p. 13, ASM International, Materials Park, OH (2000).
16. S. D. Senturia, *Microsystem Design*, p. 69, Kluwer Academic Publishers, Boston (2001).
17. D. A. Danner and D. W. Hess, *J. Appl. Phys.*, **59**, 940 (1986).
18. A. M. Efremov, D. P. Kim, and C. I. Kim, *Thin Solid Films*, **435**, 232 (2003).
19. A. M. Efremov, D. P. Kim, and C. I. Kim, *J. Vac. Sci. Technol. A*, **21**, 1568 (2003).
20. I. W. Rangelow and H. Loschner, *J. Vac. Sci. Technol. B*, **13**, 2394 (1995).
21. I. W. Rangelow, *J. Vac. Sci. Technol. A*, **21**, 1550 (2003).
22. R. A. Gottscho, C. W. Jurgensen, and D. J. Vitkarage, *J. Vac. Sci. Technol. B*, **10**, 2133 (1992).